Cohort-mean measured macromolecules lead to more robust linear-combination modeling than subject-specific or parameterized ones

Helge J. Zöllner[1,2,*], Christopher W. Davies-Jenkins[1,2], Saipavitra Murali-Manohar[1,2], Tao Gong[3,4], Steve C. N. Hui[1,2], Yulu Song[1,2], Weibo Chen[5], Guangbin Wang[3,4], Richard A. E. Edden[1,2], Georg Oeltzschner[1,2]

[1] Russell H. Morgan Department of Radiology and Radiological Science, The Johns Hopkins University School of Medicine, Baltimore, MD, United States
[2] F. M. Kirby Research Center for Functional Brain Imaging, Kennedy Krieger Institute, Baltimore, MD, United States
[3]Departments of Radiology, Shandong Provincial Hospital Affiliated to Shandong First Medical University, Jinan, Shandong, 250021,China
[4]Departments of Radiology, Shandong Provincial Hospital, Cheeloo College of Medicine, Jinan, Shandong, 250021,China
[5]Philips Healthcare, Shanghai, China

***Corresponding author:**

Helge Jörn Zöllner, Ph.D.

Division of Neuroradiology, Park 365

The Johns Hopkins University School of Medicine

600 N Wolfe St

Baltimore, MD 21287

hzoelln2@jhmi.edu

Word count: 6062

Figure count: 6

Key words: Linear-combination modeling, short-TE MRS, macromolecules, aging

Abbreviations: linear-combination modelling – LCM, macromolecular – MM, Akaike information criterion – AIC, measured MM – mMM, parameterized MM – pMM, posterior cingulate cortex – PCC, full-width half-maximum – FWHM, Hankel singular value decomposition – HSVD, total macromolecules – tMM, linear mixed-effect model – LME, Inter-class correlation coefficients – ICC, spline baseline – spbl.

Graphical Abstract

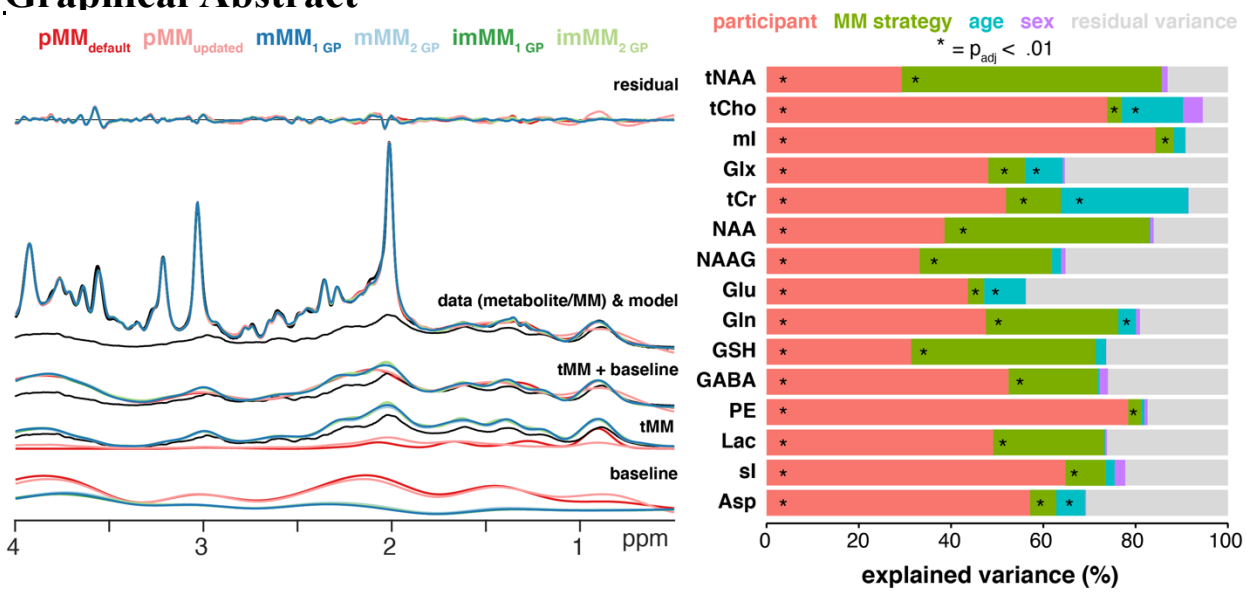

Linear-combination modeling results of short-TE PRESS from a 100-subject healthy aging cohort using different strategies to model macromolecular signals (parameterized vs measured) analyzed with Osprey. The choice of MM strategy accounts for a majority of the observed variance in the metabolite estimates for tNAA and GSH.

Abstract

Expert consensus recommends linear-combination modeling (LCM) of proton MR spectra with sequence-specific simulated metabolite basis function and experimentally derived macromolecular (MM) basis functions. Measured MM basis functions have been derived from metabolite-nulled spectra averaged across a small cohort. The use of subject-specific instead of cohort-averaged measured MM basis functions has not been studied. Furthermore, measured MM basis functions are not widely available to non-expert users, who commonly rely on parameterized MM signals internally simulated by LCM software. To investigate the impact of the choice of MM modeling, this study, therefore, compares metabolite level estimates between different MM modeling strategies (cohort-mean measured; subject-specific measured; parameterized) in a lifespan cohort and characterizes its impact on metabolite-age associations.

102 conventional (TE = 30 ms) and metabolite-nulled (TI = 650 ms) PRESS datasets, acquired from the medial parietal lobe in a lifespan cohort (20-70 years of age), were analyzed in Osprey. Short-TE spectra were modeled in Osprey using six different strategies to consider the macromolecular baseline. Fully tissue- and relaxation-corrected metabolite levels were compared between MM strategies. Model performance was evaluated by model residuals, the Akaike information criterion (AIC), and the impact on metabolite-age associations.

The choice of MM strategy had a significant impact on metabolite level estimates. The estimates agreed relatively well between different MM strategies ($r > 0.6$) and had no major impact on the variance. The lowest relative model residuals and AIC values were found for the cohort-mean measured MM. Metabolite-age associations were consistently found for two major singlet signals (tCr, tCho) for all MM strategies, but varied substantially for highly J-coupled metabolites. A variance partition analysis indicated that up to 44% of the total variance was related to the choice of MM strategy. Additionally, the variance partition analysis reproduced the metabolite-age association for tCr and tCho found in the simpler correlation analysis.

In summary, the inclusion of a single high-SNR MM basis function (cohort-mean) leads to more robust metabolite estimation (lower model residuals and AIC values) compared to MM strategies with more degrees of freedom (Gaussian parametrization) or subject-specific MM information.

Integration of multiple LCM analyses into a single statistical model potentially improves the robustness in the detection of underlying effects (e.g. metabolite vs age), reduces algorithm-based bias, and estimates algorithm-related variance.

Introduction

Single-voxel proton MRS allows in vivo research studies of brain metabolism[1,2], most commonly using PRESS localization[3]. At clinical field strength (≤3T), spectral modeling is hampered by poor spectral resolution as, particularly for short-echo-time (short-TE) spectra, metabolite signals overlap with a broad background consisting of fast-decaying macromolecule and lipid signals. Linear-combination modeling (LCM) is the consensus-recommended quantification method for short-TE spectra. LCM algorithms estimate spectra as a linear combination of metabolite and macromolecular (MM) basis function, maximizing use of prior knowledge to constrain the model solution[4].

Recent consensus on the modeling of short-TE spectra emphasizes that the MM basis functions included in the LCM must be well-parameterized separate MM basis functions based on experimentally derived MM spectra, or a single experimentally derived MM basis function should be included[4,5]. However, acquiring MM spectra is time-consuming and technically challenging especially for non-expert researchers. This results in two common practices in the field, either: 1) MM spectra are measured in a small number of subjects and then averaged into a cohort-mean MM basis function to be included in the analysis of the whole cohort and subsequent studies[5]; or 2) MM spectra are modeled using a default empirical parameterization as a series of Gaussians [6] as described in the most widely used LCM algorithm LCModel[7,8]. The latter approach is more commonly taken, especially by non-expert users, although it is not clear how adequate such parametrizations are.

Interestingly, it has not been investigated whether including subject-specific measured MMs (mMM) in the LCM has advantages over cohort-mean mMMs, possibly because prohibitively long acquisition times have disincentivized such a study, and current MRS analysis software does not provide easily accessible workflows to do so. A recent large-scale lifespan cohort[9,10] now provides sufficient publicly available data to compare the two strategies. This dataset further allows investigation of other important issues of MM modeling in short-TE spectra to be investigated:

1. Parameterized vs. measured MM: Only a few low-n studies have systematically compared metabolite estimation between parameterized MM (pMM) and mMM modeling, or studied updated MM parameterizations[11–13].
2. Other studies focused on individual differences between measured MM spectra, but did not investigate the impact on the metabolite estimation[9,14].
3. LCM algorithms apply modeling parameters to the basis functions, including a single Gaussian linebroadening parameter to account for B_0 inhomogeneities in the MRS volume[7,15,16]. This practice becomes problematic when simulated metabolite basis functions are combined with a measured MM background, since the latter already has in-vivo linewidth. It might therefore be more appropriate to use two separate Gaussian linebroadening parameters (one for metabolites, one for MM).

The overarching goal of this study was to systematically investigate different strategies for the inclusion of MM signals for linear-combination modeling of short-TE PRESS spectra, most notably the use of single-subject MM data. We sought to substantiate expert-consensus recommendations on MM handling[4,5] and provide readily usable workflows for all strategies in our analysis pipeline 'Osprey'[15]. To this end, different MM modeling strategies were implemented and applied to a large lifespan dataset from healthy volunteers[9,10]. Macromolecular modeling strategies include cohort-mean and subject-specific measured macromolecules, the most commonly used Gaussian parametrizations, and the use of a single or two separate Gaussian linebroadening parameters. In the absence of a 'gold standard', the performance of each strategy was evaluated by comparing descriptive statistics of metabolite estimates, Akaike information criteria (AIC), model residuals, and variance partition analysis. Finally, we investigated whether the choice of MM model had an influence on the observation of metabolite-age associations.

Methods

Study participants & data acquisition

In this study, a cohort of 102 healthy volunteers was recruited with equal numbers of male and female participants in each decade of life—the 20s to 60s—following local IRB approval (Shandong Hospital, China, Provincial Hospital). Exclusion criteria included a history of neurological or psychiatric illness, and contraindications for MRI. Details of the acquisition protocol can be found in published studies of the same cohort[9,10]. Briefly, all participants were scanned on a Philips 3T MRI scanner (Ingenia CX, Philips Healthcare, The Netherlands) and the protocol included a T_1-weighted MP-RAGE scan with 1 mm^3 isotropic resolution for voxel positioning and tissue segmentation. Short-TE metabolite data were acquired using PRESS localization[3] (TR/TE 2000/30 ms, 30x26x26mm^3, 96 transients, 2048 datapoints, 2000 kHz sampling bandwidth, VAPOR water suppression[17]) in the posterior cingulate cortex (PCC). Subcutaneous lipid adjacent to the voxel was suppressed with a slice-selective saturation pulse (20 mm thickness). Additionally, metabolite-nulled MM data were acquired in the same voxel with an inversion time of 650 ms using an adiabatic hyperbolic-secant inversion pulse with a full-width half-maximum (FWHM) of 698 Hz applied at 1.9 ppm to minimize impact on the water signal, which was suppressed using Philips CHESS water suppression[18]. Water reference spectra were acquired for each participant without water suppression or pre-inversion.

Data analysis

Pre-processing

Data were analyzed in MATLAB (MATLAB R2022a, The MathWorks Inc., Natick, Massachusetts, United States) using Osprey (v.2.2.0), an end-to-end open-source MRS analysis toolbox. Pre-processing on the scanner included coil-combination, averaging, and eddy-current-correction using the water reference scan[19]. Residual water signal in the metabolite and metabolite-nulled spectra was removed with a Hankel singular decomposition (HSVD) filter[20]. As previously described[9], imperfectly-nulled metabolite signals in MM spectra were removed with a linear-combination modelling procedure using simulated metabolite signals (NAA, Cr, Cho, Glu) and a highly flexible spline baseline (0.1 ppm knot spacing) to model the metabolite spectrum between 0.5 and 4.2 ppm. The fitted metabolite signals were subsequently subtracted from the spectra to

yield 'clean' MM spectra. Finally, the clean MM spectra were modeled with a flexible spline model (again 0.1 ppm knot spacing) to generate a noise-free MM basis function for subsequent LCM of the metabolite spectra (**Supplementary Material 1**).

Short-TE linear-combination modeling strategies

Metabolite data were modeled using the Osprey LCM algorithm, using a basis set of 18 metabolite basis functions generated from a fully-localized 2D density-matrix simulation of a 101 x 101 spatial grid (field of view 50% larger than voxel) implemented in the cloud-based MATLAB toolbox 'MRSCloud'[21] derived from FID-A[22]. The following metabolites were included: ascorbate, aspartate, creatine, negative creatine methylene (-$CrCH_2$), GABA, glycerophosphocholine (GPC), glutathione (GSH), Gln, Glu, mI, Lac, NAA, NAAG, phosphocholine, phosphocreatine, phosphoethanolamine (PE), Scyllo (sI), and taurine (**Figure 1**). Detailed descriptions of the frequency-domain LCM algorithm and parameter settings can be found elsewhere. Briefly, metabolite spectra were analyzed between 0.5 and 4 ppm with a spline baseline knot spacing of 0.4 ppm (recommended setting for LCM of short-TE MRS in Osprey). Model parameters of Osprey's frequency-domain LCM algorithm include amplitude estimates for the metabolite basis functions, frequency shifts, zero/first order phase correction, Gaussian and Lorentzian linebroadening, and cubic spline baseline coefficients. Water reference data were modeled with a simulated water basis function and a 6-parameter model (amplitude, zero- and first-order phase, Gaussian and Lorentzian linebroadening, and frequency shift).

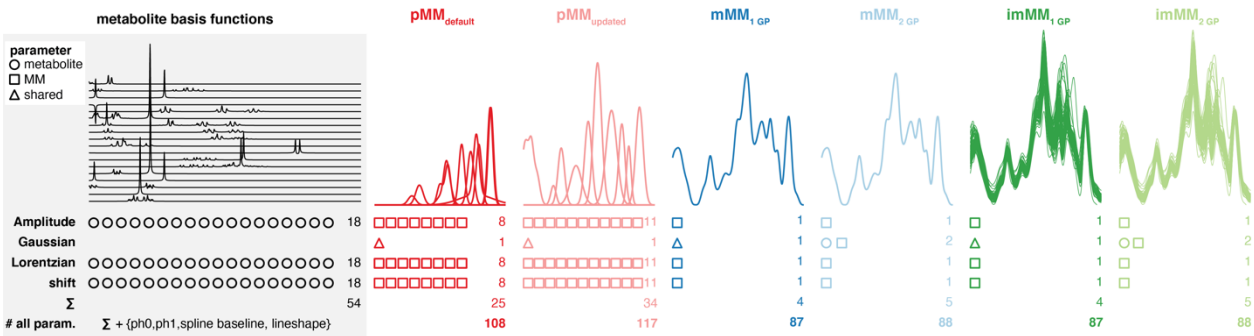

Figure 1 – Strategies to include macromolecules in the LCM of short-TE MRS, including commonly used default ($pMM_{default}$ in bold red), updated Gaussian parameterization ($pMM_{updated}$ in light red) based on measured MM spectra, single measured MM based on the cohort mean ($mMM_{1\ GP}$ and $mMM_{2\ GP}$ in bold and light blue, respectively), and individual measured MM

($imMM_{1\ GP}$ and $imMM_{2\ GP}$ in bold and light green, respectively). Inclusion of a single Gaussian model parameter for metabolites is marked "1 GP" and models using separate parameters are marked "2 GP". The number of model parameters, and indicators whether those are shared between metabolite and MM basis *functions* (triangle) or separate (circle and square respectively for metabolite and MM) are shown below.

The centerpiece of this study is the comparison of different implementations to account for MMs in short-TE LCM (**Figure 1**). In general, each MM basis function has its own model parameters for the amplitude, frequency shift, Lorentzian linebroadening. The six strategies can be grouped into 'parameterized MM' (pMM) and 'measured MM' (mMM) strategies, and the mMM strategies have been implemented with one shared or two separate Gaussian linebroadening parameters for metabolites and MM:

- The default parametrization $\mathbf{pMM_{default}}$ model (**bold red**) contains 8 Gaussian basis functions to parameterize the MMs as defined in the LCModel manual[8]. Detailed amplitudes, frequency shifts, linewidth, and soft constraints for the LCM can be found in **Supplementary Material 2**. This approach is still the most widely used implementation and its performance has previously been described for a large multi-site dataset[6].
- The updated parametrization $\mathbf{pMM_{updated}}$ model (**light red**) incorporates a total of 11 MM basis functions which are generated by averaging the spline model of all metabolite-nulled spectra and modeling that as a linear combination of 14 Gaussian peaks - between 0.5 and 4.2 ppm - with the initial frequency shifts, as previously described[9]. The resulting Gaussian basis functions between 3.7 and 4.2 ppm were summed to generate a single '$MM_{3.7\text{-}4.0}$' basis function. Again, detailed parametrization can be found in **Supplementary Material 2**.
- The cohort-mean measured $\mathbf{mMM_{1\ GP}}$ model (**dark blue**) has a single MM basis function generated by averaging the noise-free metabolite-nulled spectra from all participants. The same shared Gaussian lineshape parameter is applied to the metabolite and the MM basis function (therefore named $mMM_{1\ GP}$). This approach has the lowest number of model parameters and benefits from high signal-to-noise by using the averaged MM spectra. However, it enforces fixed ratios between the MM signals and is unable to capture any subject-specific variation of the MM signals. This approach has previously been

employed in the same cohort[10] and closely corresponds to the MRS data analysis consensus recommendations[4,5].

- The cohort-mean measured **$mMM_{2\ GP}$** model (**light blue**) is identical $mMM_{1\ GP}$, except that two Gaussian lineshape parameters are included to separately model additional linewidth applied to metabolite basis functions and the MM basis function.
- The individual subject-specific measured **$imMM_{1\ GP}$** (**dark green**) uses the noise-free metabolite-nulled spectrum from each individual subject, instead of the cohort-averaged MM basis function. This strategy incorporates subject-specific MM variation.
- The subject-specific measured **$imMM_{2\ GP}$** model (**light green**) implements the same subject-specific MM basis function with separate Gaussian lineshape parameters applied to metabolite and MM basis functions.

All models are implemented in Osprey v2.2.0 and freely available on GitHub[23]. A summary page following the MRS in MRS consensus paper[24] can be found in **Supplementary Material 3**.

Quantification, visualization, and statistics

Quantification

Water-referenced metabolite concentrations were calculated using tissue-specific water visibility and relaxation based on literature values[25,26] for each segmented tissue fraction of the voxel derived from the SPM12-based co-registration and segmentation of the T_1-weighted anatomical image and the MRS voxel[27].

Visualization

The model performance and spectral characteristics arising from the systematic differences of each modeling strategy were visually assessed through the mean spectra, mean fit model, mean total MM (tMM) models, mean spline baseline, mean total background (tMM + spline baseline), and mean residuals (means taken across all datasets).

Metabolite estimates are visualized as raincloud plots[28] with median, 25th and 75th percentile ranges, individual estimates, smoothed distributions, mean and standard deviation to identify systematic differences between the modeling strategies. The corresponding coefficients of variation

(CV) are reported as bar plots. Correlations between metabolite estimates derived using the different approaches were reported as bar plots representing Pearson's correlation coefficient, *r*. In addition, a correlation matrix comparing the correlation between the participant age and the metabolite/MM estimates for all different approaches was created. The correlation matrix includes Pearson's correlation coefficients, *r*. For significant associations, the directionality of the correlation is encoded as a color-coded ellipsoid, with higher associations represented by a narrower ellipsoid, i.e. a circle indicates there is no association (r = 0) and a line indicates perfect association (r = 1), additionally emphasized by the size of the ellipsoid (small ellipsoid ≡ small r). Associations that are significant after applying Bonferroni correction are further marked with bold font treating each MM strategy as a separate analysis (resulting in a correction factor of 15). All plots and statistics were generated in R[29] (Version 4.1.3) in RStudio (Version 2022.02.01, Build 461, RStudio Inc.) using SpecVis[6], an open-source package to visualize linear-combination modeling results with the ggplot2 package[30]. All scripts and results are publicly available on the Open Science Framework[31].

Statistics

Differences in the mean and the variance of the metabolite level estimates were assessed between $pMM_{default}$ and all other MM strategies. The statistical tests were set up as paired without any further inference. Fligner-Killeen's test with a post-hoc pair-wise Bonferroni corrected Fligner-Killeen's test was employed to test differences in metabolite estimate variance. An ANOVA, or Welch's ANOVA (depending on whether variances were different or not) was employed to test differences in the means. Post-hoc analysis was performed with a paired t-test using non-equal or equal variances, respectively.

Variance partition analysis with linear mixed-effect model

Linear mixed-effect (LME) models were set up as a repeated-measure analysis to determine variance partition coefficients to assess the contribution of MM strategy-, age-, sex- and participant-related contributions to the total variance of metabolite estimates as described previously[6,32–34]. Age and sex were defined as fixed effects while MM approach and participant were defined as random effects. The probability of observing the test statistic was evaluated against the null hypothesis, which was simulated by performing parametric bootstrapping (10,000 simulations)[35].

The resulting p-values were corrected for multiple comparison using the Benjamini-Yekutieli approach[36] which is less conservative than a Bonferroni correction, taking into account the dependency between the metabolite level estimates.

Model evaluation criteria

The performance of each modeling approach was evaluated using several metrics including the impact on the metabolite estimates, metabolite-age associations, as well as several quality metrics:

1. Visual inspection: Mean model, residual, spline baseline, tMM, and background were assessed for characteristic spectral features.
2. Consistency of metabolite estimates: between-subject coefficients of variation (CV = SD/mean) for all metabolite estimates were calculated for each modeling approach. Between-subject CV was interpreted as a measure of modeling performance, assuming that increased CVs are mainly introduced by variability in the modeling and do not reflect biological meaningful variance of metabolite estimates.
3. Agreement in the metabolite estimation between the different modeling approaches were assessed via a correlation analysis.
4. Amplitude fit quality: The difference between the maximum and minimum of the residual was determined, and then normalized by the noise level[2]. This was done over the entire modeling range and termed relative residual.
5. AIC: The Akaike information criterion[37], which takes the number of model parameters into account, is defined as follows:

$$logLikelihood_i = -0.5 * (\log(2 * \pi) + 1 - \log(N_i) + \log(SSE_i/N_i))$$

$$AIC_i = -2 * logLikelihood_i + 2K_i$$

Here, N_i is the number of points in the ith modeling strategy, SSE_i is the sum of squared error (i.e., squared residual) of that strategy, and K_i is the number of free model parameters for that strategy. In contrast to our recent study, no further corrections for amplitude soft-constraints were employed. Lower AIC_i values indicate a more

appropriate model. Subsequently, $\boldsymbol{\Delta AIC_i}$ scores were calculated as the difference of AIC_i of modeling strategy *i* and the model with the lowest AIC_{min}:

$$\Delta AIC_i = AIC_i - AIC_{min}$$

6. Inter-class correlation coefficients (ICC) were calculated between the clean MM spectra and the tMM model from the metabolite spectra LCM, as well as the clean MM spectra and the sum of tMM and spline baseline (spbl) model for all subjects.
7. Age-metabolite and age-MM associations were assessed for all models to identify interactions between differences in the model attributing signal to metabolites, MM, or spline baseline, as well as possible bias in a specific approach.
8. LME models were used to determine variance partitions for MM strategy, age, sex, participant, and residual unexplained variance which allows to make inferences about all effects across all datasets and determine influential factors in the quantitative analysis of large-cohort data.

Results

All 102 datasets were successfully processed and modeled. After further analysis, one subject was removed due to a large visible ethanol signal and a second subject was removed due to un-wanted out-of-volume echoes leading to a final total of 100 datasets. The data quality assessment indicated consistently high spectral quality (SNR_{NAA} = 151 ± 23; LW_{NAA} = 6.7 ± 0.9 Hz) without lipid contamination.

Visualization of modeling

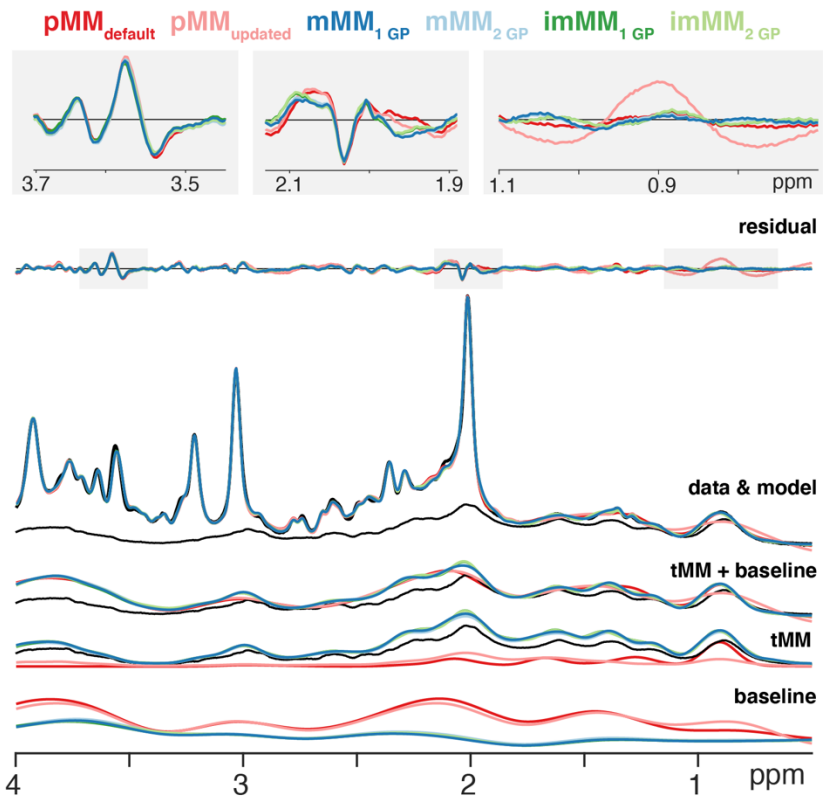

Figure 2 – Mean modeling results for all modeling strategies. Data and model agree well for all strategies; however, a substantial structured residual is apparent at 0.9 ppm for the $pMM_{updated}$ strategy. All six models are summarized with the mean results for residual, data (short-TE metabolite and MM), model, total MM model (tMM) + spline baseline model, tMM model, and spline baseline model. In addition, the mean of the 'clean' MM spectra is shown in black for reference. Three frequency regions with the largest residuals are magnified in the inlays at the top.

A summary of the data and modeling results is presented in **Figure 2**. Overall, a strong agreement between the mean of data and model is found for all modeling strategies. However,

there is a substantial structured signal in the mean residual at 0.9 ppm for the $pMM_{updated}$ strategy, indicating non-optimal parametrization of the $MM_{0.93}$ peak. The mean of the sum of the MM and baseline models agree well across all strategies, indicating that the combination of these two terms achieves comparable modeling of all broad non-metabolite signals, although the pMM strategies exhibit a broader and differently shaped signal in the 2-ppm region compared to the mMM strategies. Of note, there appears to be no systematic difference between the cohort-mean and the subject-specific mMM strategies, or between the strategies using 1 or 2 Gaussian linebroadening parameters. Upon closer inspection, it becomes strikingly obvious that the main differences appear between the pMM and mMM strategies, particularly with regard to how much signal they attribute to the baseline and the MM model, respectively, i.e. all pMM strategies attribute a lot more signal to the baseline model. In contrast, the mMM strategies exhibit a much flatter baseline model, and closely follow the shape of the mean mMM signal (except for a small scaling factor related to the different relaxation experienced by the MM between the metabolite-nulled and the metabolite spectra). Interestingly, the $pMM_{default}$ strategy agrees well with the mMM strategies at 0.9 ppm, but substantially less in the remaining frequency regions. The smaller residual could be related to an overparameterization in this region, as two separate Gaussians ($MM_{0.91}$ & $Lip_{0.89}$) are included at 0.9 ppm for this strategy. The mean spline baseline models of the parameterized strategies have a higher number of more pronounced peaks (1.4, 2.2, 3.0, and 3.7 ppm) compared to the experimentally derived strategies indicating that the LCM algorithm estimates a larger portion of the overall signal as baseline for the former strategies.

Metabolite level estimates: Distribution and Correlation

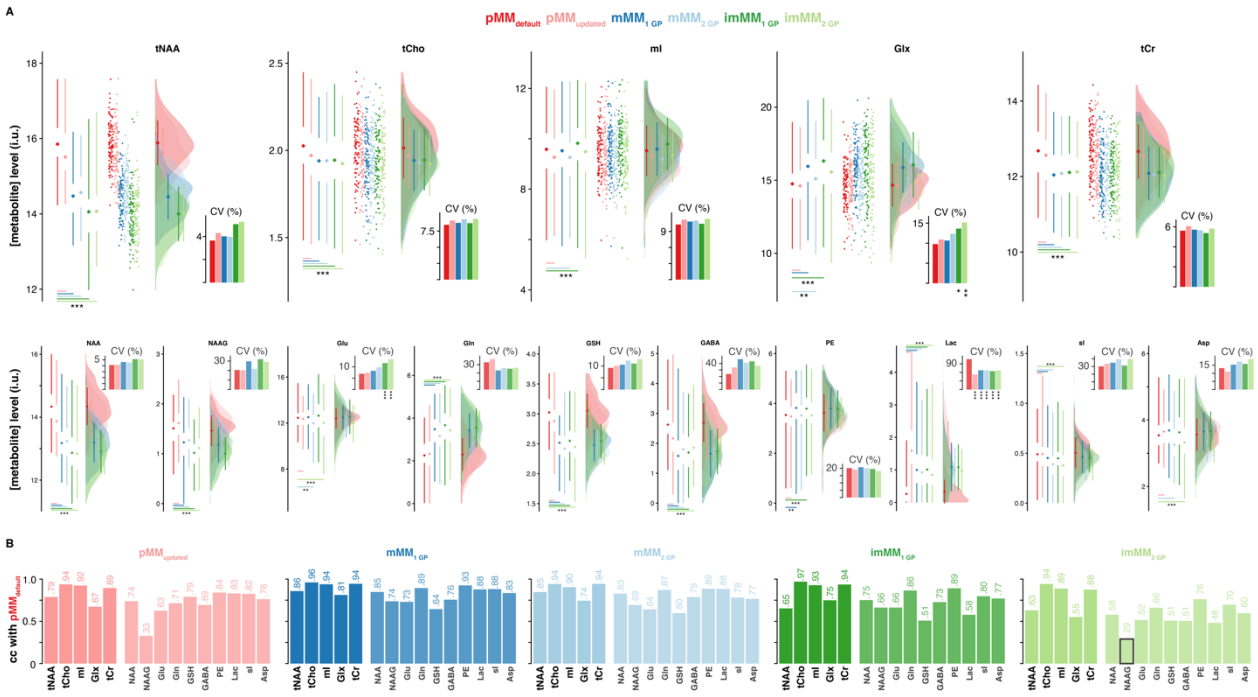

Figure 3 – Metabolite level estimates distribution and correlation between MM strategies. (A) Metabolite estimate distributions major metabolites (first row) and other metabolites (second row not including individual data points) for all MM strategies. For the raincloud plots, box plots with median, interquartile range, and 25th/75th percentile, individual data points, smoothed distributions, and mean with standard deviation are shown. The bar plot inlays show the corresponding CV values. Asterisks indicate significant differences in the mean or variance (adjusted $p < 0.05$ = *, adjusted $p < 0.01$ = **, adjusted $p < 0.001$ = ***). (B) Pearson's correlation coefficient, r, for the correlation analysis between the $pMM_{default}$ and all other MM strategies. All correlations were found to be significant except for the one outlined in black.

A summary analysis of the metabolite level estimates is shown in **Figure 3** and summarized in **Table 1**. Significant differences in mean metabolite level estimates between the 'default parametrization' strategy $pMM_{default}$ and any other strategy were found for almost all metabolites (**Figure 3A**). Most notably, these include reductions in tNAA, separate NAA and NAAG, tCr and GSH. A notable significant increase in the metabolite levels compared to the default parametrization strategy was found for Glx which is mainly driven by changes in the Gln estimates. No overall trend for the variance of the metabolite level estimates was observed. A significant increase in the variance was found for some of the metabolites when using subject-specific measured MM spectra, including Glx ($imMM_{1\ GP}$, $imMM_{2\ GP}$), and Glu ($imMM_1$

$_{GP}$,imMM$_{2\ GP}$). This is potentially a result of the low SNR of individual MM spectra causing unwanted variance during the removal of residual metabolite signal during the MM clean-up. Lactate metabolite level estimates are substantially reduced (likely removing overestimation in the default parametrization strategy) and exhibit less variance for the mMM strategies (**Figure 3A** second row). In general, a strong correlation ($r > 0.6$) was found between the pMM$_{default}$ strategy and all other strategies for almost all metabolites (**Figure 3B**). Particularly strong associations were found for metabolites with strong singlet signals (tNAA, tCr, and tCho) or with no observable signal in the MM spectra. For J-coupled metabolites whose residual contributions are difficult to reliably and accurately remove from the MM spectra (i.e. Glu and Gln), a weaker association between strategies was found. Supporting this notion, the agreement between strategies for highly J-coupled metabolites (GSH, and NAAG) was generally lower since the complex multiplet signals of these metabolites are more difficult to reliably distinguish from the broad background. The introduction of separate Gaussian linewidth parameters for metabolites and MM resulted in lower concentration estimates for 13 out of 30 metabolites, unchanged concentrations for 13 out of 30 metabolites and higher concentrations for 4 out of 30 metabolites when compared to the MM strategies with a single shared Gaussian linewidth parameter and two separate Gaussian linewidth parameter . Metabolites with strong singlet signals were not affected by this, except for tNAA, driven primarily by changes in the NAAG level estimation. Interestingly, the direction of change when introducing a second Gaussian parameter was similar for both the mMM and imMM strategies. No change of metabolite level variance were observed for the 2 GP strategies for the majority of metabolites (28 out of 30 comparisons). However, a significant variance reduction was observed for lactate level estimates when a separate Gaussian linewidth parameter was introduced.

Table 1 – Summary of the descriptive statistics of the metabolite level estimates. In each case, the upper number is the mean metabolite concentration and the lower italic number is the standard deviation of the metabolite concentration across all subjects. Significant differences in mean or variance between a specific MM strategy and the pMM$_{default}$ strategy are marked in bold.

metabolite	pMM$_{default}$	pMM$_{updated}$	mMM$_{1\ GP}$	mMM$_{2\ GP}$	imMM$_{1\ GP}$	imMM$_{2\ GP}$
tNAA	15.89 *0.58*	**15.60** *0.67*	**14.45** *0.58*	**14.59** *0.58*	**14.00** *0.71*	**14.02** *0.74*
tCho	2.01 *0.17*	**1.97** *0.18*	**1.94** *0.17*	**1.93** *0.18*	**1.95** *0.17*	**1.92** *0.18*

mI	9.53 *0.98*	**9.29** *1.04*	9.59 *1.04*	**9.18** *1.01*	**9.79** *1.02*	9.35 *1.06*
Glx	14.66 *1.43*	**14.59** *1.59*	**15.86** *1.69*	**15.13** *1.87*	**16.06** ***2.19***	15.37 ***2.33***
tCr	12.66 *0.71*	**12.53** *0.76*	**12.09** *0.69*	**12.05** *0.68*	**12.11** *0.65*	**12.03** *0.70*
NAA	14.34 *0.59*	**13.95** *0.58*	**13.19** *0.61*	**13.23** *0.60*	**12.91** *0.66*	**12.84** *0.65*
NAAG	1.46 *0.30*	**1.58** *0.32*	**1.18** *0.35*	**1.29** *0.28*	**1.00** *0.32*	**1.10** *0.32*
Glu	12.42 *0.86*	**12.32** *0.91*	12.48 *1.03*	**11.96** *1.17*	12.55 ***1.46***	**11.97** ***1.60***
Gln	2.29 *0.75*	2.32 *0.85*	**3.43** *0.79*	**3.21** *0.83*	**3.55** *0.89*	**3.44** *0.90*
GSH	3.05 *0.28*	**2.89** *0.29*	**2.47** *0.26*	**2.44** *0.30*	**2.54** *0.28*	**2.48** *0.32*
GABA	2.69 *0.64*	**2.21** *0.75*	**1.65** *0.77*	**1.83** *0.75*	**1.73** *0.75*	**1.90** *0.69*
PE	3.63 *0.73*	**3.45** *0.66*	**3.80** *0.79*	3.56 *0.71*	**3.78** *0.74*	3.59 *0.65*
Lac	0.33 *0.35*	**1.64** ***0.86***	**1.09** ***0.73***	**1.00** ***0.67***	**1.08** ***0.69***	**0.98** ***0.65***
sI	0.50 *0.15*	**0.48** *0.16*	**0.46** *0.16*	**0.38** *0.15*	0.45 *0.14*	**0.38** *0.15*
Asp	3.56 *0.47*	**3.63** *0.40*	3.65 *0.56*	**3.35** *0.58*	3.67 *0.58*	**3.36** *0.63*

Model evaluation criteria

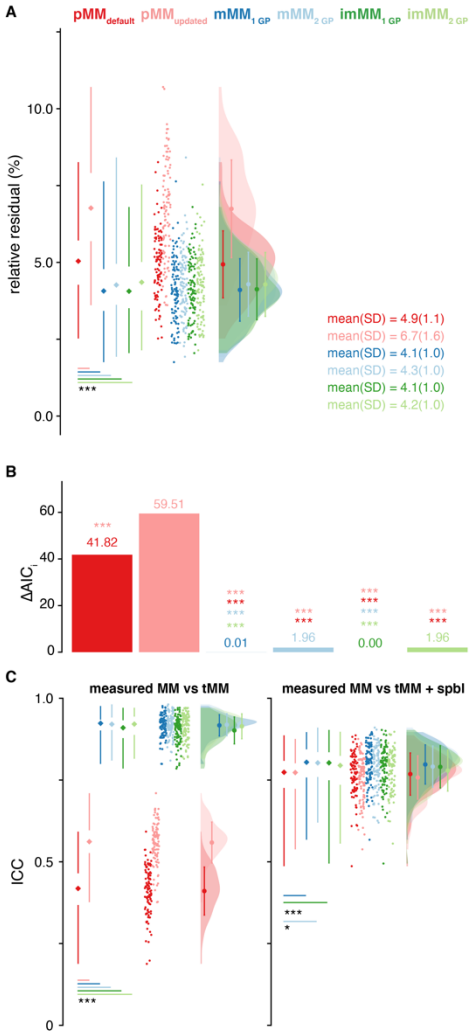

Figure 4 – Secondary analysis of residuals, and agreement between short-TE LCM total MM (tMM) model and individual MM spectra. Lower residual amplitudes and AIC scores were found for experimentally derived MM strategies. (A) Relative residual (%) for all MM strategies. (B) Mean ΔAIC values for all MM strategies. Asterisks indicate significant differences (adjusted $p < 0.001$ = ***) between a specific pair of MM strategies (color-coded). (C) ICC between the individual's MM data and the short-TE LCM tMM or tMM + spbl model of the same individual. Asterisks indicate significant differences (adjusted $p < 0.05$ = *, adjusted $p < 0.001$ = ***).

The results of the model evaluation criteria in terms of model residual, AIC, and agreement between short-TE LCM tMM model and individual MM spectra are shown in **Figure 4**. A significant reduction of the model residual was found for all mMM strategies compared to the pMM strategies (**Figure 4A**). Surprisingly, this suggests that an accurate representation (mMM and

imMM) with fewer of degrees of freedom outperforms generalized representations (pMM) with a higher number of degrees of freedom. The $imMM_{1\ GP}$ strategy resulted in the overall lowest AIC, therefore, it was taken as the reference (AIC_{min}) for the ΔAIC calculation (**Figure 4B**). However, no significant difference in the AIC was found between the subject-specific $imMM_{1\ GP}$ and cohort-mean $mMM_{1\ GP}$ strategies, indicating comparable parsimony for both strategies. A significant but small increase in the ΔAIC value was found for the strategies with separate Gaussian linewidth parameters for metabolites and MM ($imMM_{2\ GP}$ & $mMM_{2\ GP}$) indicating that the possible advantage of one additional linewidth parameter was not justified by sufficiently high improvements of the model residual. Both parameterized strategies resulted in significantly higher ΔAIC values relative to the experimentally derived strategies due to the larger number of MM components and higher degree of freedom without offering lower model residuals than the mMM and imMM strategies.

The ICC analysis (**Figure 4C**) substantiates observations from Figure 2, i.e. poor agreement between the short-TE LCM tMM model estimated by the pMM strategies and the 'ground-truth' measured MM data. This indicates that the LCM performs relatively well in separating metabolite and broader background signals, however, it is unable to distinguish between spline spectral baseline and MM signals, especially for the pMM strategies. When the sum of the MM and baseline models is considered, the agreement with the measured MM background improves, but remains significantly poorer for $pMM_{default}$ compared to 3 out of 4 measured MM strategies ($mMM_{1\ GP}$, $mMM_{2\ GP}$, $imMM_{1\ GP}$).

Effect on metabolite-age associations

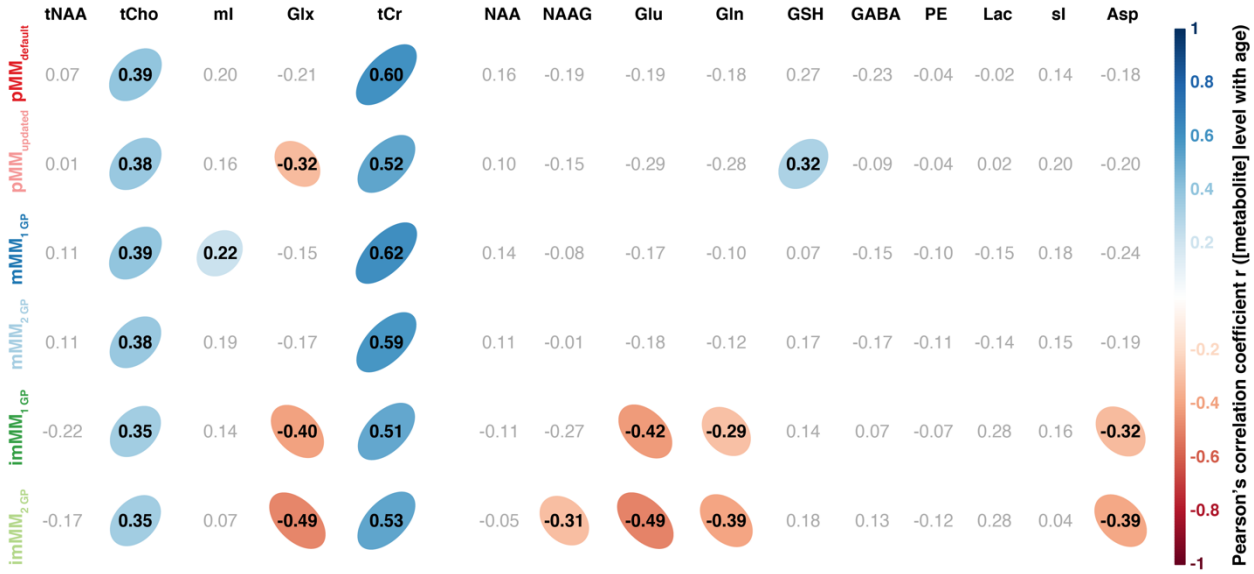

Figure 5 – Secondary analysis of metabolite-age associations for all MM strategies. Correlation matrix of Pearson's correlation coefficient, r, for the metabolite-age association. Results indicate stable metabolite-age associations for the major singlet metabolites, but more variable results for metabolites with stronger J-coupling. Significant correlations are indicated with bold letters and color-coded ellipsoids with the directionality of r indicated by color and orientation and magnitude of r by the size of the ellipsoid. Bonferroni correction is employed for each MM strategy separately (correction factor of 15 metabolite level estimates).

The metabolite-age associations for all MM strategies are summarized in a correlation matrix in **Figure 5**. The two strong positive correlations between metabolite level and age for the two major singlet metabolites tCho (*r* between 0.35 and 0.39) and tCr (*r* between 0.51 and 0.62) are stable across all MM strategies with the strongest association found for the $mMM_{1\ GP}$ strategy. Metabolite-age associations are more variable between MM strategies for highly J-coupled metabolites that are affected by the characterization of the MM background for the frequency region > 3.2 ppm (see $MM_{3.7\text{-}4.0}$ age association in **Supplementary Material 4**). This is especially apparent for mI (*r* between 0.07 and 0.22), Glx (r between -0.15 and -0.49, affecting Glu and Gln similarly), NAAG (*r* between -0.01 and -0.31), and GSH (*r* between 0.07 and 0.32). It is worth noting that changes in the tCr association may impact the interpretation if creatine ratios are reported. Studies investigating age-related changes in metabolites markers of interest in aging (such as GSH) may reach differing conclusions depending on the MM modeling approach (although, note that quantification of GSH with LCM at 3T is controversial). Similar to the changes for > 3.2

ppm frequency region, the variability in the non-significant correlation of age and tNAA may be explained by signal contributions in the 2 ppm frequency region being attributed to the MM or baseline (see $MM_{2.0}$ age association in **Supplementary Material 4**), especially as the $MM_{2.0}$ component is significantly associated with age for the pMM strategies.

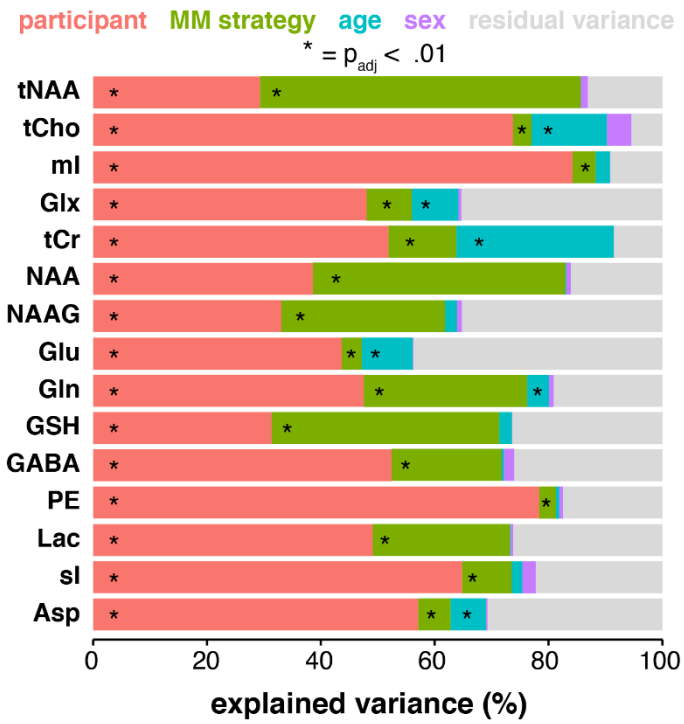

Figure 6 – Variance partition analysis for each metabolite across all MM strategies. The linear-mixed effect model includes fixed effects for age and sex, and random effects for participant and MM strategy. Significant effects are marked with an asterisk (adjusted $p < 0.01$ = *).

The variance partition analysis is summarized in **Figure 6** and **Table 2**. For most metabolites, the largest portion of the variance is explained by the participant level, representing biological variance between subjects. However, the choice of MM strategy explains a significant portion of the observed metabolite level variance for all metabolites and is a stronger variance contributor than 'participant' for tNAA (56.3% vs 29.4%), NAA (44.4% vs 38.6%), and GSH (40% vs 31.4%). In addition, 43.7% of the variance of Glu is not explained by any of the included factors. Comparing this analysis, which combines all results in a single analysis, with the simpler correlation analysis separated by MM strategy (Figure 5) confirms some of the metabolite-age associations. For example, tCr and tCho show a strong impact of age, which was also consistently found

across all MM strategies in the correlation analysis. In contrast to the correlation analysis, the LME analysis also indicates significant contributions of age effects for Glx, Glu, Gln, and Asp which were found only for a subset of MM strategies in the correlation analysis. Further, no variance contribution from age was found for mI, NAAG, and GSH, which were in turn observed in the correlation analysis.

Table 2 - Variance partition estimation for each metabolite across all MM strategies. The linear-mixed effect model includes fixed effects for age, and sex and random effects for participant and MM strategy. Significant effects are marked with an asterisk (adjusted $p < 0.01$ indicated in bold).

metabolite	participant	MM strategy	age	sex	residual
tNAA	**29.4**	**56.3**	0	1.2	13.1
tCho	**73.8**	**3.2**	**13.3**	4.3	5.4
mI	**84.3**	**4.0**	2.5	0	9.2
Glx	**48.1**	**8.0**	**8.2**	0.5	35.3
tCr	**51.9**	**11.9**	**27.6**	0.1	8.5
NAA	**38.6**	**44.4**	0.2	0.8	16.1
NAAG	**33.1**	**28.8**	2.0	0.9	35.2
Glu	**43.7**	**3.5**	**9.0**	0.1	43.7
Gln	**47.6**	**28.7**	**3.8**	0.9	19
GSH	**31.4**	**40.0**	2.2	0.1	26.3
GABA	**52.5**	**19.3**	0.4	1.8	26
PE	**78.4**	**2.9**	0.6	0.7	17.4
Lac	**49.1**	**24.1**	0.1	0.4	26.2
sI	**64.8**	**8.7**	1.9	2.3	22.2
Asp	**57.1**	**5.7**	**6.2**	0.2	30.7

Discussion

We have presented a comparison of six different strategies to incorporate MM basis functions into short-TE LCM metabolite estimation applied to a large lifespan cohort. The major goals were: 1) to compare metabolite level estimates obtained with cohort-mean and subject-specific measured MM and different MM parametrizations; 2) to identify potential sources of differences between the strategies and how they affect metabolite-age associations. The key findings of our study are:

- Group-mean metabolite level estimates significantly differ between parameterized and experimentally derived MM strategies, most notably for tNAA, tCr and GSH. However, for most metabolites, the estimate variance did not change.
- Despite differences in the mean, metabolite estimates correlated strongly ($r > 0.6$) between the default MM parametrization strategy $pMM_{default}$ and all other MM strategies. Highly J-coupled metabolites showed weaker correlations between MM strategies than singlet signals.
- Experimentally derived MM strategies performed better in terms of residuals and parsimony metrics than parameterized strategies, indicating higher agreement between data and model. This is especially intriguing since measured MM models have a lower number of model parameters and therefore fewer degrees of freedom, and are less prone to overfitting compared to the parameterized strategies.
- Metabolite-age associations were relatively stable across MM strategies for metabolites with major singlet signals, however, less so for highly J-coupled metabolites. Variance partition analysis indicated that up to 56.3% (tNAA) of metabolite level variance can be explained by the choice MM strategy. This highlights the importance of choosing an appropriate MM modeling strategy, and its impact on validity and interpretation of the results. The variance partition analysis further substantiated the metabolite-age associations for tCho, tCr, Glx, Glu, and Gln. Incorporating the choice of different modeling strategies into a global analysis may increase the robustness of its findings compared to a single correlation analysis.

In this study we took advantage of Osprey's modularity and accessible LCM algorithm to create a workflow for directly incorporating subject-specific MM spectra and to introduce separate

Gaussian linebroadening parameters for metabolites and MM. These novel modifications highlight a key strength of open-source LCM workflows, since they would be much more tedious (if not outright impossible) to do in closed-source or pre-compiled LCM algorithms. Our results did not demonstrate any substantial advantage conferred by the use of subject-specific MM data – on the contrary, metabolite estimates for tNAA and Glx actually increased, and did not find substantial differences introduced by an additional Gaussian linebroadening parameter for MM. This suggests that cohort-mean MM basis functions can be used in homogeneous populations. It remains unclear how many participants' worth of MM data would constitute a cohort-representative MM spectrum, though. A potentially interesting strategy could be a short metabolite-nulled acquisition in every single participant to generate one robust cohort-specific averaged MM spectrum instead of one long metabolite-nulled acquisition in only a few subjects. The significant impact of the choice of MM modeling strategy on short-TE LCM has been shown in several earlier studies[11–13]. Although these studies are either not performed at clinically relevant field strength (≤3T) or their statistical power is limited[11–13], we found evidence to support a number of their key findings. Confirming previous reports by Schaller et al.[11] using the LCModel algorithm[7], we found a significant increase in Glx estimates when using experimentally derived MM, however, in contrast to their results, this effect was dominated by increased Gln estimates while Glu remained unaffected. We further substantiated their findings that NAA and tNAA estimates decrease when using measured MMs or an updated MM parametrization. This is mostly related to the differences in the amplitude of the $MM_{2.0}$ peak which is notably smaller in the $pMM_{default}$ strategy than in all mMM spectra. However, it remains unclear whether the large 2-ppm signals in the mMM data represent 'real' MM contributions, are an artifact of the residual metabolite clean-up process of the MM, or still contain metabolite signals not accounted for during the clean-up process. A recently presented method using strongly diffusion-weighted MRS to determine the MM background yielded much smaller $MM_{2.0}$ signals, more distinct MM peaks in the 3.5 to 4 ppm region, and narrower lines in general[38] compared to the IR method used in our study or previously used SR methods[14]. It is unclear which of the approaches is more appropriate and less error-prone to estimate the MM background. Another, similar study by Gottschalk et al.[12] reported comparable changes in size and directionality using the QUEST LCM algorithm[39]. Confirming findings from that study, we found evidence for a substantial advantage of the experimentally-derived MM strategies over parameterized approaches for the quantification of lactate,

which is typically a very small signal on the shoulder of a broad MM peak around 1.3 ppm[12]. Both studies conclude that effects they observe are unlikely to affect the outcome in MRS application studies, however, there is no analysis directly proving this assumption. Both studies featured comparably small samples (11 for Schaller et al., and 20 for Gottschalk et al.) from a narrow age range, which is a substantial limitation to the generalizability of their findings to clinical and age-related studies. In contrast, we studied the impact of the MM strategy choice in a large cohort across the lifespan and unequivocally showed a major influence on the observed metabolite-age associations, especially for highly J-coupled metabolites with strong relevance in aging (e.g. GSH).
A third study by Hofmann et al.[14] used a saturation-recovery-based method to measure metabolite and MM spectra simultaneously including 40 healthy subjects with three age groups (< 25, 25-55, >55 years), but did not report metabolite quantification results.

In comparison to the most widely used LCM algorithm, LCModel, Osprey's algorithm uses an unregularized spline baseline model, no prior distributions for the Lorentzian lineshape parameters, and single Gaussian MM basis functions for the parameterized approach. Therefore, the advantages of using a single MM basis function may be more pronounced for this less constrained implementation, as it strongly reduces the parameter space for the LCM algorithm. This additionally explains the relatively poor performance of the $pMM_{updated}$ strategy, e.g., for the $MM_{0.91}$ peak as the updated strategy does only include a single basis function around 0.90 ppm as opposed to two for the $pMM_{default}$ strategy ($MM_{0.92}$ & $Lip_{0.9}$). Additionally, the original LCModel algorithm includes range of frequencies and FWHM for the Gaussian peaks, as well as expectation values for the Lorentzian lineshape parameters which introduce more freedom to the algorithm to model those signals compared to Osprey. Thus, it would be interesting but beyond the scope of this study to perform the same comparison with LCModel, or compare different LCM algorithms as previously done but with the measured MM spectra. It is possible that the introduction of a regularized baseline, such as the one described in LCModel, or more advanced baseline approaches as implemented in ABFit[40] or elsewhere[13] could improve the performance of parameterized MM estimation during short-TE LCM and allow for separation of metabolite, MM, and baseline signals. Apart from regularization terms, the flexibility of a spline baseline can also be controlled by the density of the spline knot spacing and is has been shown to have major impact

on the quantification[41,42]. This is especially the case if separate Gaussian MM basis functions are used. In this study, we used Osprey's default spbl knotpsacing of 0.4 ppm which resulted in reasonable baseline flexibility for the experimentally derived MM strategies and a good agreement in the combined tMM + spbl model for all strategies. However, we could potentially further improve the performance of the experimentally derived MM strategies as the underlying MM signals are sufficiently described by the single MM basis function.

In comparison to metabolite spectra, MM spectra have much broader, smaller, low-SNR and are relatively featureless, which makes them extremely difficult to characterize and model appropriately. Since they are routinely derived from single-inversion recovery experiment and metabolites differ in their T_1 relaxation behavior, experimental MM spectra will contain contributions from imperfectly nulled metabolite signals. These need to be removed to generate pure MM spectra ("clean-up"), but the removal process is far from straightforward, and the low SNR of subject-specific experimental MM prevents perfect removal with sufficient certainty. While there were no visually striking residual metabolite signals in the MM spline model, the higher variance of tNAA and Glx estimates for the subject-specific imMM strategies suggests that imperfectly cleaned-up residual metabolite signals in the single-subject MM spectra contribute variability and uncertainty. One contributing factor to this might be T1 differences between moieties, and the use moiety-specific basis functions during clean-up might reduce residual metabolite signals. accounting for. On the acquisition side, saturation-recovery[14] or double-inversion recovery approaches might achieve improve the consistency of metabolite nulling, however, at the cost of greater T_1-weighting of the MM signals. To reduce T_1-weighting effects diffusion-weighted metabolite-nulling could be used which is less susceptible to T_1 differences from different metabolites or introduced by aging[38]. Finally, the MM derived with metabolite nulling will differ from the MM background in the metabolite spectra by a T_1 relaxation factor. This is accounted for during LCM with a single linear amplitude scaling parameter for the MM basis function. While this is consensus-recommended best practice, it obviously requires the assumption that all MM signals relax with the same T_1, which may not be justified.

Perspective for extension of multi-LCM approaches

This study is, to the best of the authors' knowledge, the first study to explicitly consider the additional variance introduced from different LCM strategies and settings in the final statistical analysis to model biological effects in the cohort, in this case metabolite-age associations. This 'meta-LCM' approach could prove to be more robust to model-based bias than a statistical analysis based on a single model, as seen in the differences observed in the separate correlation matrix. A novel generalized LCM analysis fully capturing model-related variance would require a large number of diverse modeling strategies. These may include different signal parametrizations (arbitrary lineshape as in Osprey[15] and LCModel[7], asymmetric lineshape as in ABFit[40], number of lineshape parameters), MM approaches (Gaussian basis functions, Voigt basis functions, mean/individually measured MM spectra), background signal descriptions (spline functions as in Osprey[15] and LCModel[7], polynomials like in FSL-MRS, subtraction techniques as in QUEST[16,45] and Tarquin), parameter regularization, and model domain (time vs frequency domain, combined time and frequency domain, real- or complex-valued data). With ever-increasing computational resources, a 'multi-model' meta-analysis could lead to more robust metabolite estimation and provide a better estimate of estimation uncertainties related to the choice of modeling strategy.

Limitations

A major limitation of the study, and in-vivo MRS in general, is the absence of a 'ground truth' of metabolite level estimates to validate LCM results against. Like in our previous studies[6,46], we evaluated the performance of the different modeling strategies from a combination of estimate variance, fit residuals, parsimony scores, and robustness of observed metabolite-age associations. However, low variance or AICs do not reflect higher accuracy and may rather indicate insufficient responsiveness to real biological variance. The use of simulated spectra as a ground truth is extremely promising as a validation strategy[47], but can only succeed if synthetic data are truly representative of in-vivo conditions. Another limitation is the single LCM algorithm that we used here, Osprey, which—while conceptually and in performance[6] similar to LCModel does not feature regularization terms on the baseline or the lineshape, and features fewer metabolite soft constraints. The data in this study are of exceptionally high spectral quality (high SNR, narrow linewidth, and no lipid contamination) and our observations and conclusions may be substantially differed for spectra of lower spectral quality (low SNR, broader linewidth, and lipid

contamination). Finally, since this study focuses on MM modeling strategies, we did not include a detailed interpretation and discussion of associations between metabolite levels, age and sex, which can be found elsewhere[10].

Conclusion

Inclusion of a single high-SNR MM basis function derived from the cohort mean of measured metabolite-nulled spectra lead to more robust metabolite estimation compared to subject-specific measured MM or Gaussian parametrizations with more degrees of freedom. While there were systematic differences of certain metabolite estimates (tNAA, Glx) between MM strategies, metabolite-age associations (particularly tCho, tCr) were relatively stable. Agreement between MM strategies was generally stronger for singlet signals than for J-coupled signals.

References

1. Öz G, Alger JR, Barker PB, et al. Clinical Proton MR Spectroscopy in Central Nervous System Disorders. *Radiology*. 2014;270(3):658-679. doi:10.1148/radiol.13130531

2. Wilson M, Andronesi O, Barker PB, et al. *Methodological Consensus on Clinical Proton MRS of the Brain: Review and Recommendations*. Vol 82. John Wiley and Sons Inc.; 2019. doi:10.1002/mrm.27742

3. Bottomley P. *Selective Volume Method for Performing Localized NMR Spectroscopy*. Vol 3.; 1985. doi:10.1016/0730-725X(85)90032-3

4. Near J, Harris AD, Juchem C, et al. Preprocessing, analysis and quantification in single-voxel magnetic resonance spectroscopy: experts' consensus recommendations. *NMR Biomed*. 2020;34:e4257. doi:10.1002/nbm.4257

5. Cudalbu C, Behar KL, Bhattacharyya PK, et al. Contribution of macromolecules to brain 1H MR spectra: Experts' consensus recommendations. *NMR Biomed*. 2021;34(5):e4393. doi:10.1002/nbm.4393

6. Zöllner HJ, Považan M, Hui SCN, Tapper S, Edden RAE, Oeltzschner G. Comparison of different linear-combination modeling algorithms for short-TE proton spectra. *NMR Biomed*. 2021;34(4):e4482. doi:https://doi.org/10.1002/nbm.4482

7. Provencher SW. Estimation of metabolite concentrations from localized in vivo proton NMR spectra. *Magn Reson Med*. 1993;30(6):672-679. doi:10.1002/mrm.1910300604

8. Provencher S. LCModel & LCMgui User's Manual. LCModel & LCMgui User's Manual. http://s-provencher.com/pub/LCModel/manual/manual.pdf. Published 2020. Accessed April 28, 2020.

9. Hui SCN, Gong T, Zöllner HJ, et al. The macromolecular MR spectrum does not change with healthy aging. *Magn Reson Med*. 2022;87(4):1711-1719. doi:10.1002/mrm.29093

10. Gong T, Hui SCN, Zöllner HJ, et al. Neurometabolic timecourse of healthy aging. *bioRxiv*. June 2022. doi:10.1101/2022.06.08.495050

11. Schaller B, Xin L, Cudalbu C, Gruetter R. Quantification of the neurochemical profile using simulated macromolecule resonances at 3 T. *NMR Biomed*. 2013;26(5):593-599. doi:10.1002/nbm.2896

12. Gottschalk M, Lamalle L, Segebarth C. Short-TE Iocalised 1H MRS of the human brain at 3T: Quantification of the metabolite signals using two approaches to account for macromolecular signal contributions. *NMR Biomed*. 2008;21(5):507-517. doi:10.1002/nbm.1219

13. Zhang Y, Shen J. Smoothness of in vivo spectral baseline determined by mean-square error. *Magn Reson Med*. 2014;72(4):913-922. doi:10.1002/mrm.25013

14. Hofmann L, Slotboom J, Boesch C, Kreis R. Characterization of the macromolecule baseline in localized 1H-MR spectra of human brain. *Magn Reson Med*. 2001;46(5):855-863. doi:10.1002/mrm.1269

15. Oeltzschner G, Zöllner HJ, Hui SCN, et al. Osprey: Open-source processing, reconstruction & estimation of magnetic resonance spectroscopy data. *J Neurosci Methods*. 2020;343:108827. doi:10.1016/j.jneumeth.2020.108827

16. Wilson M, Reynolds G, Kauppinen RA, Arvanitis TN, Peet AC. A constrained least-squares approach to the automated quantitation of in vivo 1H magnetic resonance spectroscopy data. *Magn Reson Med*. 2011;65(1):1-12.

17. Tkáč I, Starčuk Z, Choi IY, Gruetter R. In vivo 1H NMR spectroscopy of rat brain at 1 ms echo time. *Magn Reson Med*. 1999;41(4):649-656. doi:10.1002/(SICI)1522-2594(199904)41:4<649::AID-MRM2>3.0.CO;2-G

18. Haase A, Frahm J, Hanicke W, Matthaei D. 1H NMR chemical shift selective (CHESS) imaging. *Phys Med Biol*. 1985;30(4):341-344. doi:10.1088/0031-9155/30/4/008

19. Klose U. In vivo proton spectroscopy in presence of eddy currents. *Magn Reson Med*. 1990;14(1):26-30. doi:10.1002/mrm.1910140104

20. Barkhuijsen H, de Beer R, van Ormondt D. Improved algorithm for noniterative time-domain model fitting to exponentially damped magnetic resonance signals. *J Magn Reson 1969*. 1987;73(3):553-557. doi:10.1016/0022-2364(87)90023-0

21. Hui SCN, Saleh MG, Zöllner HJ, et al. MRSCloud: a Cloud-based MR Spectroscopy Tool for Basis Set Simulation. March 2022:2022.03.22.485310. doi:10.1101/2022.03.22.485310

22. Simpson R, Devenyi GA, Jezzard P, Hennessy TJ, Near J. Advanced processing and simulation of MRS data using the FID appliance (FID-A)—An open source, MATLAB-based toolkit. *Magn Reson Med*. 2015;77(1):23-33. doi:10.1002/mrm.26091

23. Osprey GitHub repository. Osprey GitHub repository. https://github.com/schorschinho/osprey. Published 2020. Accessed May 27, 2020.

24. Lin A, Andronesi O, Bogner W, et al. Minimum Reporting Standards for in vivo Magnetic Resonance Spectroscopy (MRSinMRS): Experts' consensus recommendations. *NMR Biomed*. 2021;34(5):e4484. doi:10.1002/nbm.4484

25. Gasparovic C, Song T, Devier D, et al. Use of tissue water as a concentration reference for proton spectroscopic imaging. *Magn Reson Med*. 2006;55(6):1219-1226. doi:10.1002/mrm.20901

26. Wansapura JP, Holland SK, Dunn RS, Ball WS. NMR relaxation times in the human brain at 3.0 Tesla. *J Magn Reson Imaging*. 1999;9(4):531-538. doi:10.1002/(SICI)1522-2586(199904)9:4<531::AID-JMRI4>3.0.CO;2-L

27. Friston K. *Statistical Parametric Mapping: The Analysis of Functional Brain Images*. Academic Press; 2007. http://books.google.com/books?id=KZZcLqkxhFIC%5Cnpapers://8fdc0079-0571-40b9-b7fa-84608563a121/Paper/p10618.

28. Allen M, Poggiali D, Whitaker K, Marshall TR, Kievit RA. Raincloud plots: a multi-platform tool for robust data visualization. *Wellcome Open Res*. 2019;4:63. doi:10.12688/wellcomeopenres.15191.1

29. R Core Team. *R: A Language and Environment for Statistical Computing*. Vienna, Austria: R Foundation for Statistical Computing; 2017. https://www.R-project.org/.

30. Wickham H. *Ggplot2: Elegant Graphics for Data Analysis*. Springer-Verlag New York; 2009. http://ggplot2.org.

31. Zöllner HJ. Cohort-mean measured macromolecules lead to more robust linear-combination modeling than subject-specific or parameterized ones. June 2022. doi:10.17605/OSF.IO/7DXNM

32. Mikkelsen M, Barker PB, Bhattacharyya PK, et al. Big GABA: Edited MR spectroscopy at 24 research sites. *NeuroImage*. 2017;159:32-45. doi:10.1016/j.neuroimage.2017.07.021

33. Mikkelsen M, Rimbault DL, Barker PB, et al. Big GABA II: Water-referenced edited MR spectroscopy at 25 research sites. *NeuroImage*. 2019;191:537-548. doi:10.1016/J.NEUROIMAGE.2019.02.059

34. Považan M, Mikkelsen M, Berrington A, et al. Comparison of Multivendor Single-Voxel MR Spectroscopy Data Acquired in Healthy Brain at 26 Sites. *Radiology*. 2020;295(1):191037. doi:10.1148/radiol.2020191037

35. Halekoh U, Højsgaard S. A Kenward-Roger Approximation and Parametric Bootstrap Methods for Tests in Linear Mixed Models The R Package pbkrtest. *J Stat Softw*. 2014;59(1):1-32. doi:10.18637/jss.v059.i09

36. Benjamini Y, Yekutieli D. The control of the false discovery rate in multiple testing under dependency. *Ann Stat*. 2001;29(4):1165-1188. doi:10.1214/aos/1013699998

37. Akaike H. A new look at the statistical model identification. *IEEE Trans Autom Control*. 1974;19(6):716-723. doi:10.1109/TAC.1974.1100705

38. Simsek K, Döring A, Pampel A, Möller HE, Kreis R. Macromolecular background signals for gray and white matter regions in the human brain as defined from strong diffusion-weighted MR spectroscopy. In: *31st Annual Meeting of the International Society for Magnetic Resonance in Medicine (ISMRM)*. London, UK; 2022.

39. Graveron-Demilly D. Quantification in magnetic resonance spectroscopy based on semi-parametric approaches. *Magn Reson Mater Phys Biol Med*. 2014;27(2):113-130. doi:10.1007/s10334-013-0393-4

40. Wilson M. Adaptive Baseline Fitting for 1H MR Spectroscopy Analysis. *bioRxiv*. February 2020:2020.02.17.949495. doi:10.1101/2020.02.17.949495

41. Giapitzakis IA, Borbath T, Murali-Manohar S, Avdievich N, Henning A. Investigation of the influence of macromolecules and spline baseline in the fitting model of human brain spectra at 9.4T. *Magn Reson Med*. 2019;81(2):746-758. doi:10.1002/mrm.27467

42. Marjańska M, Terpstra M. Influence of fitting approaches in LCModel on MRS quantification focusing on age-specific macromolecules and the spline baseline. *NMR Biomed*. November 2019:e4197. doi:10.1002/nbm.4197

43. Murali-Manohar S, Wright AM, Borbath T, Avdievich NI, Henning A. A novel method to measure T1-relaxation times of macromolecules and quantification of the macromolecular resonances. *Magn Reson Med*. 2021;85(2):601-614. doi:10.1002/mrm.28484

44. Murali-Manohar S, Borbath T, Wright AM, Soher B, Mekle R, Henning A. T2 relaxation times of macromolecules and metabolites in the human brain at 9.4 T. *Magn Reson Med*. 2020;84(2):542-558. doi:10.1002/mrm.28174

45. Poullet JB, Sima DM, Simonetti AW, et al. An automated quantitation of short echo time MRS spectra in an open source software environment: AQSES. *NMR Biomed*. 2007;20(5):493-504. doi:10.1002/nbm.1112

46. Zöllner HJ, Tapper S, Hui SCN, Barker PB, Edden RAE, Oeltzschner G. Comparison of linear combination modeling strategies for edited magnetic resonance spectroscopy at 3 T. *NMR Biomed*. 2021:e4618. doi:10.1002/nbm.4618

47. Marjańska M, Deelchand DK, Kreis R, Team the 2016 IMSGFC. Results and interpretation of a fitting challenge for MR spectroscopy set up by the MRS study group of ISMRM. *Magn Reson Med*. 2022;87(1):11-32. doi:10.1002/mrm.28942

Declaration of competing interests

The authors have nothing to declare.

Acknowledgement

This work is supported by NIH grants P41 EB015909, R01 EB016089, and R01 EB023963 R21A G060245. GO receives support from NIH grant K99 AG062230.

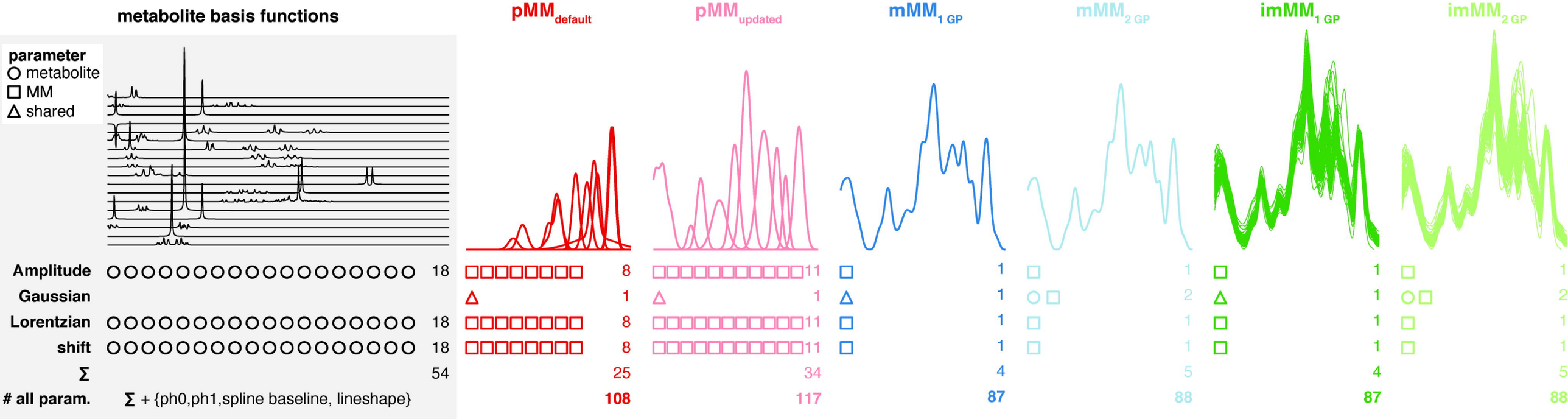
metabolite basis functions
pMM default
pMM updated
mMM 1 GP
mMM 2 GP
imMM 1 GP
imMM 2 GP
parameter
metabolite
MM
shared
Amplitude 18 8 11 1 1 1 1
Gaussian 1 1 1 2 1 2
Lorentzian 18 8 11 1 1 1 1
shift 18 8 11 1 1 1 1
Σ 54 25 34 4 5 4 5
all param. Σ + {ph0,ph1,spline baseline, lineshape} 108 117 87 88 87 88

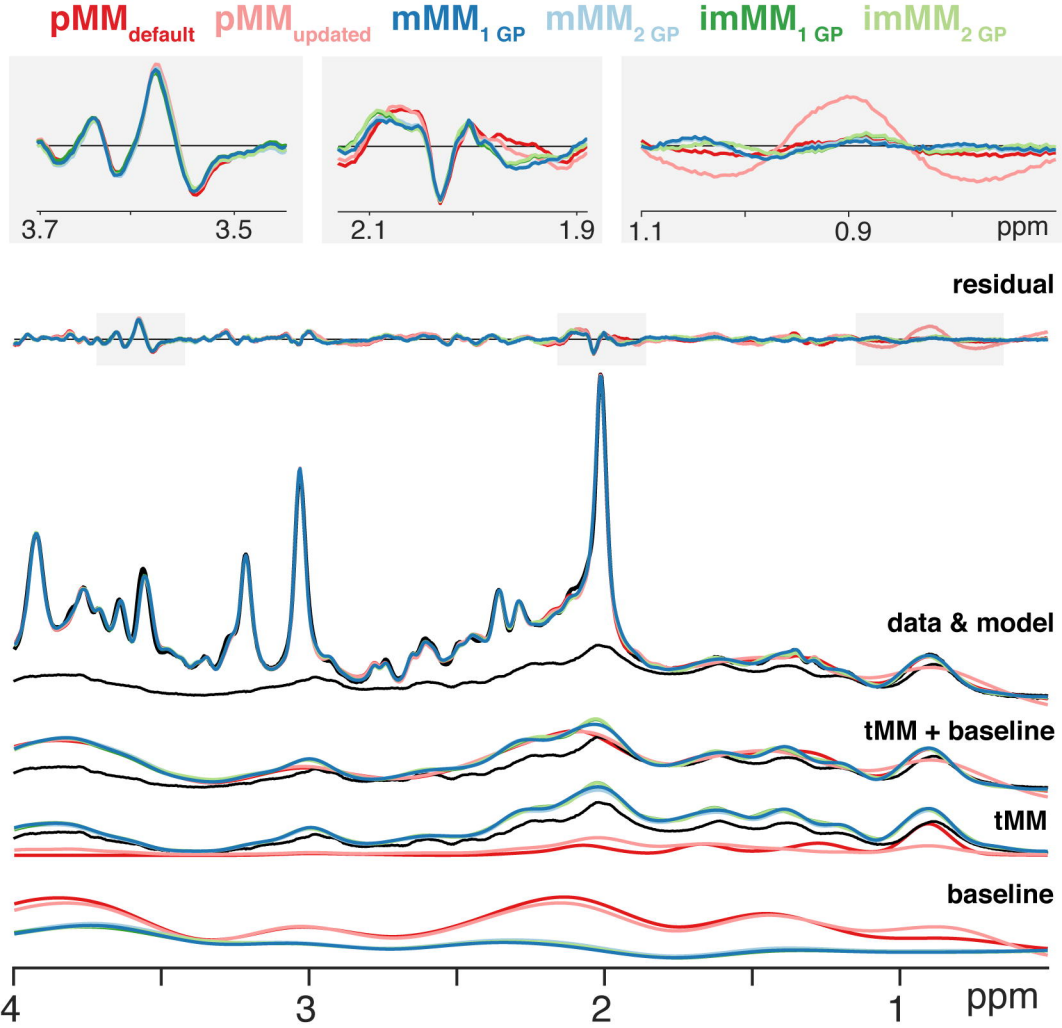
pMM default
pMM updated
mMM 1 GP
mMM 2 GP
imMM 1 GP
imMM 2 GP
3.7
3.5
2.1
1.9
1.1
0.9
ppm
residual
data & model
tMM + baseline
tMM
baseline
4
3
2
1
ppm

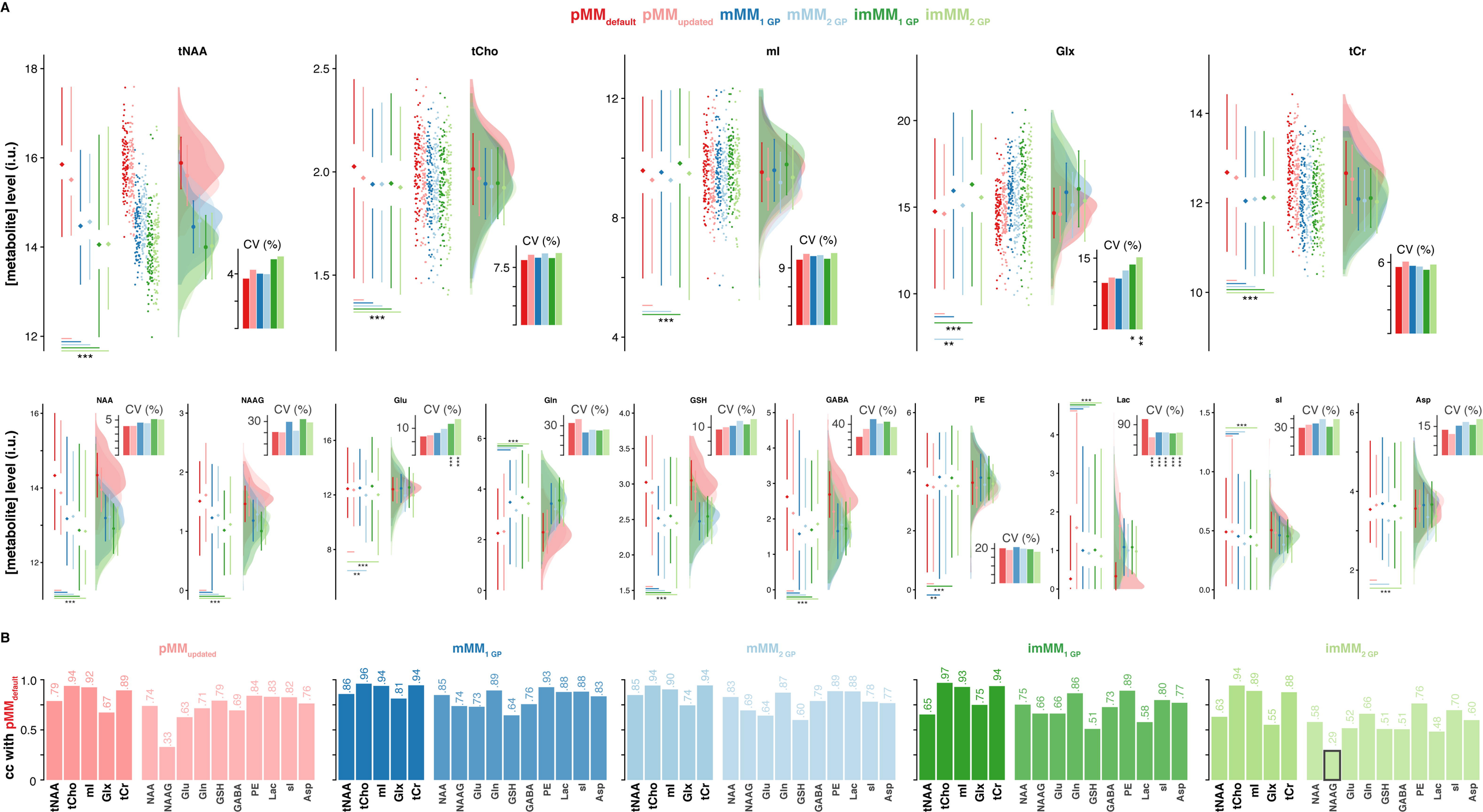
A
pMM default
pMM updated
mMM 1 GP
mMM 2 GP
imMM 1 GP
imMM 2 GP
tNAA
tCho
mI
Glx
tCr
[metabolite] level (i.u.)
CV (%)
NAA
NAAG
Glu
Gln
GSH
GABA
PE
Lac
sI
Asp
B
cc with pMM default
pMM updated
mMM 1 GP
mMM 2 GP
imMM 1 GP
imMM 2 GP

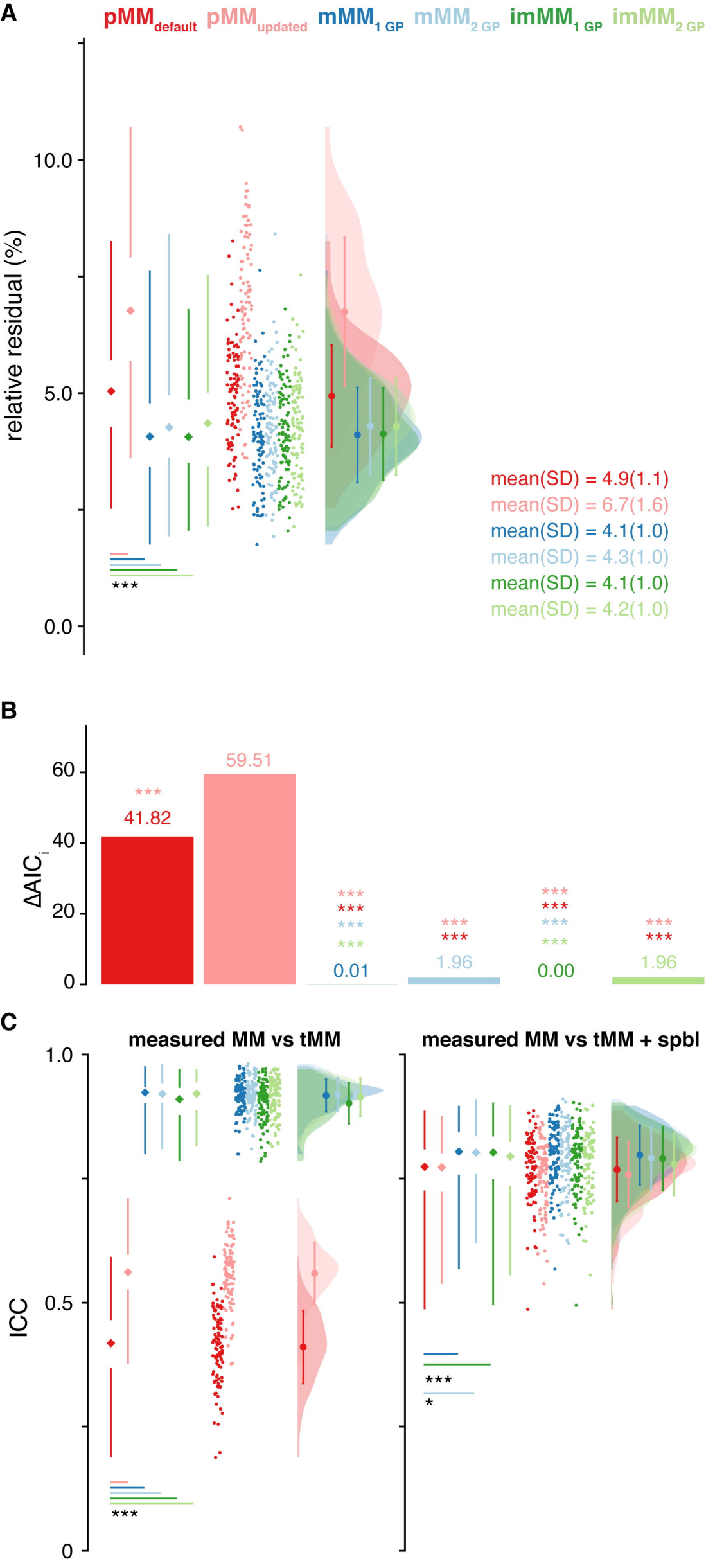
A
pMM default
pMM updated
mMM 1 GP
mMM 2 GP
imMM 1 GP
imMM 2 GP
relative residual (%)
10.0
5.0
0.0
***
mean(SD) = 4.9(1.1)
mean(SD) = 6.7(1.6)
mean(SD) = 4.1(1.0)
mean(SD) = 4.3(1.0)
mean(SD) = 4.1(1.0)
mean(SD) = 4.2(1.0)
B
ΔAIC_i
60
40
20
0
***
41.82
59.51
***
***
***
***
0.01
***
***
1.96
***
***
***
***
0.00
***
***
1.96
C
measured MM vs tMM
measured MM vs tMM + spbl
ICC
1.0
0.5
0
***
***
*

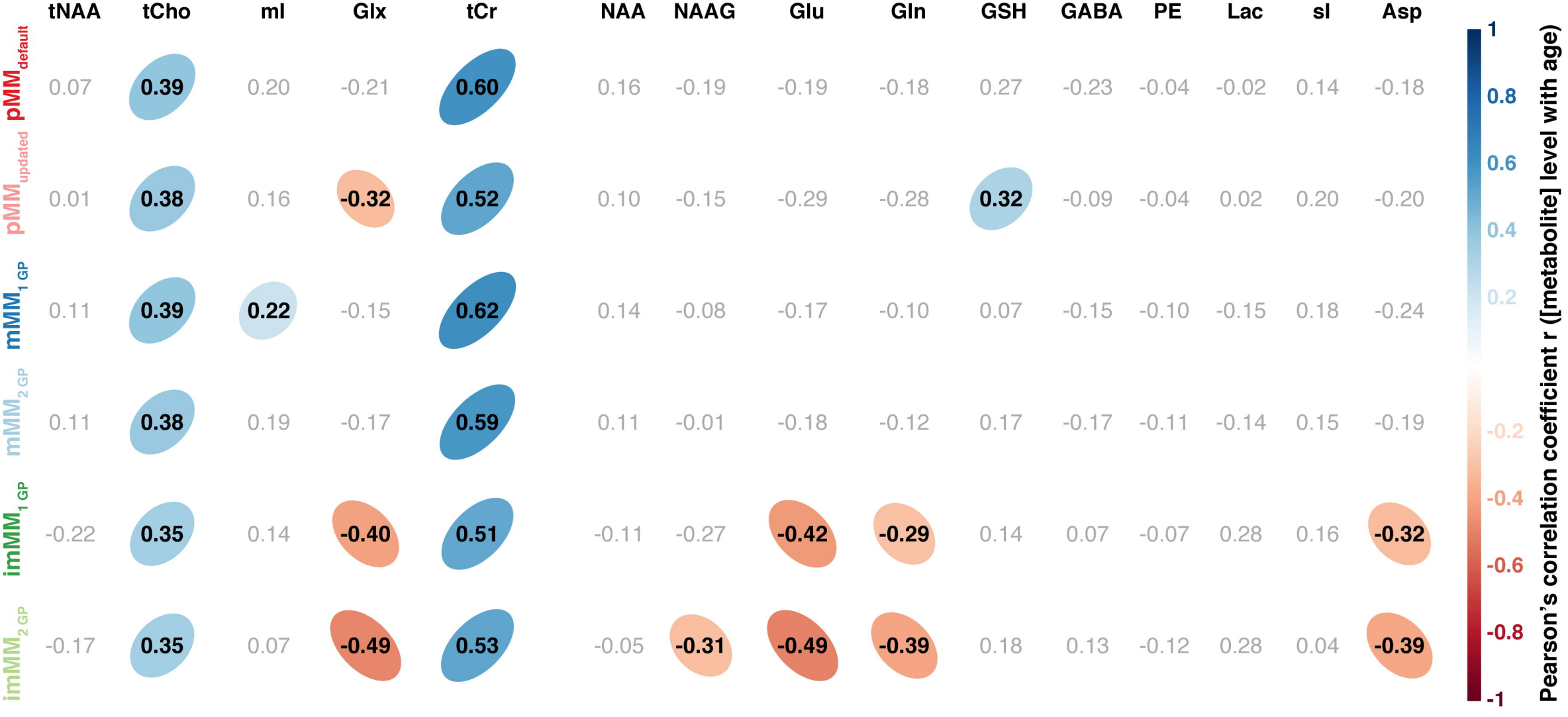
tNAA tCho mI Glx tCr NAA NAAG Glu Gln GSH GABA PE Lac sI Asp
pMM default
0.07 0.39 0.20 -0.21 0.60 0.16 -0.19 -0.19 -0.18 0.27 -0.23 -0.04 -0.02 0.14 -0.18
pMM updated
0.01 0.38 0.16 -0.32 0.52 0.10 -0.15 -0.29 -0.28 0.32 -0.09 -0.04 0.02 0.20 -0.20
mMM 1 GP
0.11 0.39 0.22 -0.15 0.62 0.14 -0.08 -0.17 -0.10 0.07 -0.15 -0.10 -0.15 0.18 -0.24
mMM 2 GP
0.11 0.38 0.19 -0.17 0.59 0.11 -0.01 -0.18 -0.12 0.17 -0.17 -0.11 -0.14 0.15 -0.19
imMM 1 GP
-0.22 0.35 0.14 -0.40 0.51 -0.11 -0.27 -0.42 -0.29 0.14 0.07 -0.07 0.28 0.16 -0.32
imMM 2 GP
-0.17 0.35 0.07 -0.49 0.53 -0.05 -0.31 -0.49 -0.39 0.18 0.13 -0.12 0.28 0.04 -0.39
1
0.8
0.6
0.4
0.2
-0.2
-0.4
-0.6
-0.8
-1
Pearson's correlation coefficient r ([metabolite] level with age)

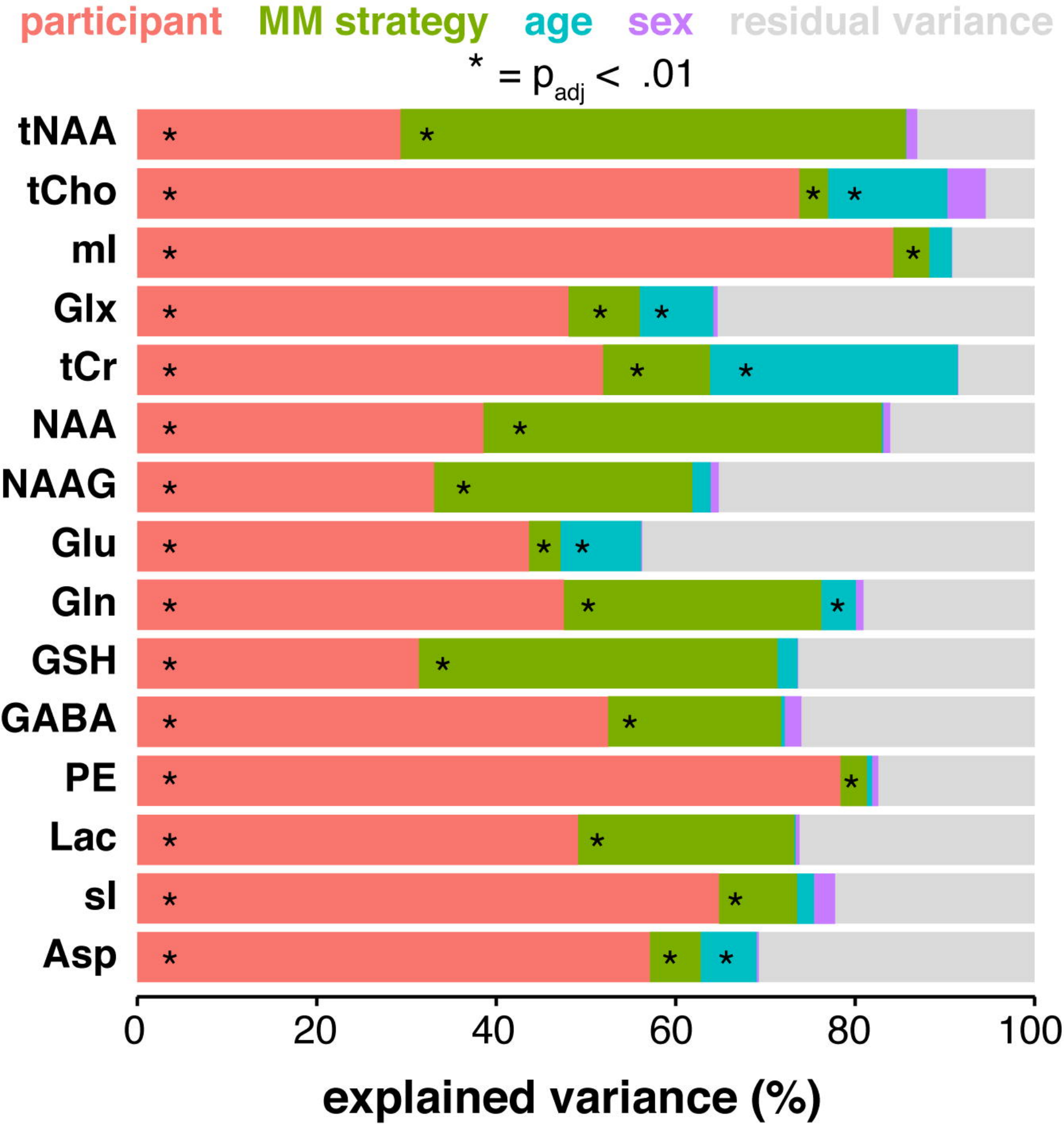
participant
MM strategy
age
sex
residual variance
* = p_adj < .01
tNAA
tCho
mI
Glx
tCr
NAA
NAAG
Glu
Gln
GSH
GABA
PE
Lac
sI
Asp
0
20
40
60
80
100
explained variance (%)

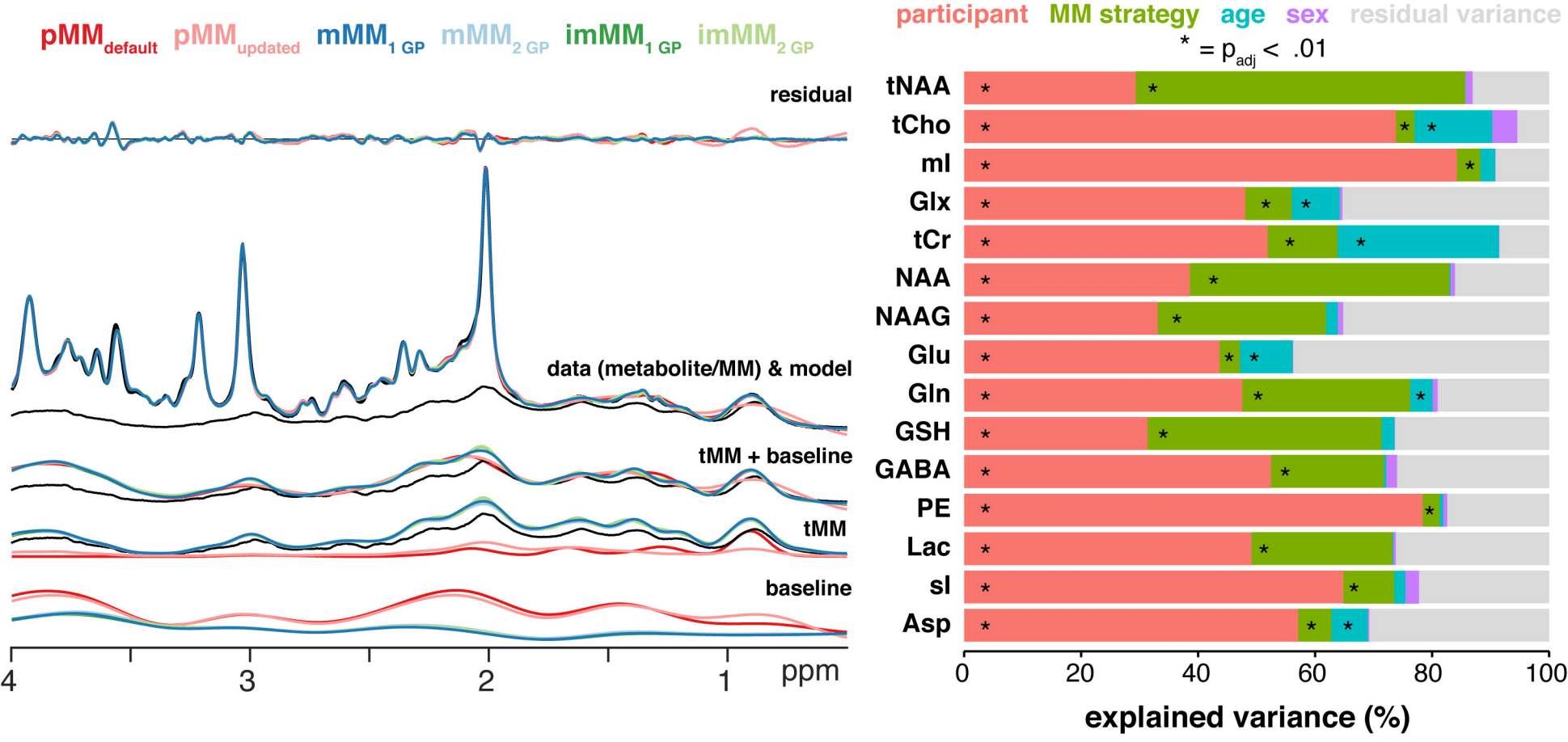
pMM default
pMM updated
mMM 1 GP
mMM 2 GP
imMM 1 GP
imMM 2 GP
residual
data (metabolite/MM) & model
tMM + baseline
tMM
baseline
4
3
2
1
ppm
participant
MM strategy
age
sex
residual variance
* = p adj < .01
tNAA
tCho
mI
Glx
tCr
NAA
NAAG
Glu
Gln
GSH
GABA
PE
Lac
sI
Asp
0
20
40
60
80
100
explained variance (%)